A three-dimensional all-metal terahertz metamaterial perfect absorber

Meng Wu, Xiaoguang Zhao, Jingdi Zhang, Jacob Schalch, Guangwu Duan, Kevin Cremin, Richard D. Averitt, and Xin Zhang

Citation: Appl. Phys. Lett. **111**, 051101 (2017); doi: 10.1063/1.4996897
View online: https://doi.org/10.1063/1.4996897
View Table of Contents: http://aip.scitation.org/toc/apl/111/5
Published by the American Institute of Physics

Articles you may be interested in

Active control and switching of broadband electromagnetically induced transparency in symmetric metadevices
Applied Physics Letters **111**, 021101 (2017); 10.1063/1.4993428

Broadband non-polarizing terahertz beam splitters with variable split ratio
Applied Physics Letters **111**, 071101 (2017); 10.1063/1.4986538

Nonlinear terahertz metamaterials with active electrical control
Applied Physics Letters **111**, 121101 (2017); 10.1063/1.4990671

Active tuning of high-Q dielectric metasurfaces
Applied Physics Letters **111**, 053102 (2017); 10.1063/1.4997301

Broadband metamaterial for optical transparency and microwave absorption
Applied Physics Letters **110**, 143511 (2017); 10.1063/1.4979543

Tunable electromagnetically induced transparency from a superconducting terahertz metamaterial
Applied Physics Letters **110**, 241105 (2017); 10.1063/1.4985618

A three-dimensional all-metal terahertz metamaterial perfect absorber

Meng Wu,[1,a),b)] Xiaoguang Zhao,[1,b)] Jingdi Zhang,[2] Jacob Schalch,[2] Guangwu Duan,[1] Kevin Cremin,[2] Richard D. Averitt,[2,c)] and Xin Zhang[1,c)]
[1]*Department of Mechanical Engineering, Boston University, 110 Cummington Mall, Boston, Massachusetts 02215, USA*
[2]*Department of Physics, University of California, San Diego, 9500 Gilman Dr., La Jolla, California 92093, USA*

(Received 6 May 2017; accepted 18 July 2017; published online 1 August 2017)

We present a three-dimensional terahertz metamaterial perfect absorber (MPA) that exhibits a high quality factor and is polarization insensitive. The unit cell is composed of two orthogonally oriented copper stand-up split ring resonators deposited on a copper ground plane with capacitive gaps in free space away from the substrate. Near unity (99.6%) absorption at ∼1.65 THz is experimentally obtained in excellent agreement with simulation results. The quality factor is ∼37, which is quite large for a terahertz MPA because of reduced material losses in the all-metal structure. According to simulation results, the MPA is insensitive to the polarization of the incident wave, and more than 90% absorption can be achieved for angles of incidence up to 60° for both TE and TM polarized incident THz waves. *Published by AIP Publishing*. [http://dx.doi.org/10.1063/1.4996897]

Electromagnetic absorber materials are useful for many applications such as light collecting for solar cells,[1,2] electro-absorption modulators,[3] detectors,[4] and energy conversion devices,[5] among others. During the past several years, metamaterials have opened up a new route to realize tailored absorbing materials.[6–8] Various metamaterial absorbers have been theoretically and experimentally investigated from microwave to visible light frequencies.[9] This also includes the terahertz (THz) region of the spectrum, which lies between the microwave and infrared frequencies spanning from ∼0.1 to 10 THz. The useful properties of THz radiations include transparency to numerous non-conducting materials that are opaque at other frequencies, distinct spectroscopic signatures of many organic materials, and their non-ionizing characteristic.[10,11] These features make the development of metamaterial perfect absorbers (MPAs) at THz frequencies attractive for applications ranging from spectroscopic identification of hazardous materials to noninvasive imaging.

Many MPAs consist of three sandwiched planar components: a layer of metamaterial resonators, a dielectric spacer layer, and a conductive ground plane.[12] The MPAs are configured to minimize the reflection and transmission of the incident wave via matching their effective impedance (Z_{eff}) to the free space, achieved by engineering the effective permittivity (ε_{eff}) and permeability (μ_{eff}) using metamaterials.[13] The absorption spectrum of a tri-layer planar MPA strongly depends on the polarization and angle of the incident wave, which is valid not only for the polarized split ring resonators (SRRs)[6] but also for the four-fold symmetric structures.[13] The origin of discrepancy between the TE and TM responses for various incident angles has been fully investigated, and the role of surface waves has been revealed.[14] Three-dimensional structures also provide an alternative route to achieve perfect absorption. For example, a three-dimensional symmetric (fish-spear-like) structure has been fabricated by using the two-photon polymerization process and surface gold coating to realize a perfect absorber at mid-infrared frequencies.[15]

Inspired by this work, we designed and fabricated a symmetric all-metal three-dimensional (3D) MPA operating at THz frequencies and investigated the electromagnetic response experimentally and using numerical simulations. An absorption of 99.6% at a fundamental resonance frequency of 1.65 THz with a high quality factor ($Q \approx 37$) is experimentally measured.

In our design, we employ the split ring resonator (SRR) as the basic element in our design. In a SRR, an oscillating current is excited at the fundamental inductive-capacitive (LC) resonance mode by an electric field polarized normal to the capacitive gap.[16,17] As opposed to a planar MPA design, we utilize a unit-cell structure composed of two identical stand-up SRRs perpendicular to one another with the capacitive gaps suspended away from the conductive ground plane, as illustrated in Fig. 1(a). This eliminates the dielectric spacer layer (and the associated uncontrolled losses), which is a crucial component in conventional planar MPAs.[18–23] From the geometry of the 3D MPA, we can see that it consists of four copper components, from bottom to top: ground plane, bottom wires, pillars, and top bars. Comparing with the four-tined fish-spear-like resonator (FFR) structure,[15] we introduce top bars in the 3D MPA to construct the unit-cells. The top bars increase the equivalent inductance and capacitance in the resonator, making the structure more compact than the FFR. In addition, the periodicity in our design is small, which strengthens the coupling between adjacent unit cells. Both increased capacitance and coupling allow stronger field confinement in the MPA, increasing the overall sensitivity to changes in the local environment. Moreover, our MPA is an all-metal structure fabricated by multi-layer electroplating processes (as described below), which is compatible with CMOS processing and is suitable for batch production.

[a)]Also at School of Mechanical Engineering, Northwestern Polytechnical University, Xi'an, China.
[b)]M. Wu and X. Zhao contributed equally to this work.
[c)]Authors to whom correspondence should be addressed: raveritt@ucsd.edu and xinz@bu.edu

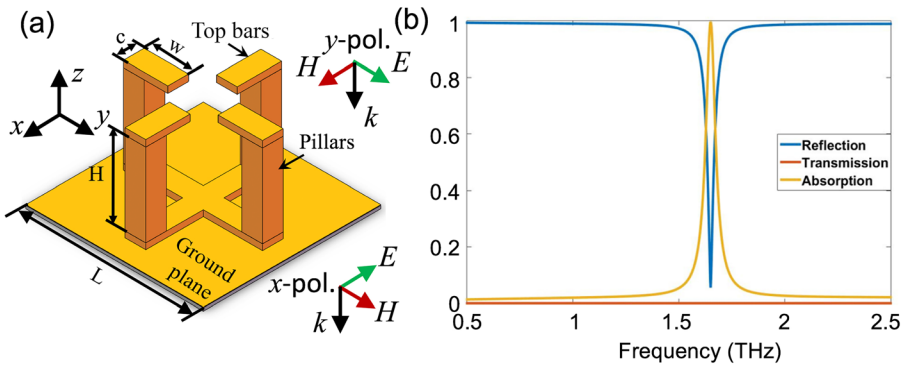

FIG. 1. (a) 3D MPA unit cell with structural parameters: L = 60 μm, H = 30 μm, c = 5 μm, and w = 15.8 μm. The thickness of the ground plane is 0.2 μm. The bottom wires and top panels are with the same thickness of 2 μm. The length of the bottom wires is 46 μm. (b) Simulation results showing reflection (R), transmission (T), and calculated absorption. The absorption (A) could be expressed as $A = 1 - R$. In simulation, a 99.9% absorption could be achieved at a resonance frequency of 1.65 THz.

An array of stand-up SRRs couples to the electric and magnetic fields of the incident THz wave. With an optimized structural design, impedance matching can be achieved at a designated frequency, leading to perfect absorption. This is shown in Fig. 1(b), which presents numerical simulation results using the frequency solver in CST Microwave Studio. In the model, copper with a conductivity of 2×10^7 S/m is utilized as the material of the MPA and periodic boundary conditions are applied. The results reveal near-unity absorption at 1.65 THz, corresponding to the fundamental resonance mode of the 3D MPA, with a quality factor (Q) of ~38.5 at normal incidence. Q is calculated as $Q = f_0/\Delta f$, where f_0 is the fundamental resonance frequency and Δf is the full width at half maximum of the absorption. The high-Q absorption results from material loss reduction by removing the dielectric spacer, which is a major source of uncontrolled material loss for tri-layer planar MPAs.[12]

We fabricated the 3D MPA by multilayer electroplating,[24] as shown in Figs. 2(a)–2(f). At first, a 200-nm-thick copper seed layer was deposited on a silicon substrate as the ground plane by e-beam evaporation [Fig. 2(a)]. Then, a 2-μm-thick photoresist of S1813 (Shipley Inc.) was spin-coated and photo-defined, followed by copper electroplating and photoresist removal [Fig. 2(b)]. Then, we patterned a layer of 30-μm-thick AZ9260 photoresist (MicroChemicals GmbH) as the mold for copper pillar electroplating [Fig. 2(c)]. Following pillar formation, another seed layer was deposited directly on top of the photoresist [Fig. 2(d)]. On the second seed layer, the photoresist of S1813 was spin-coated and photo-defined, followed by electroplating of the top bars [Fig. 2(e)]. Finally, the photoresist and second seed layer were removed to obtain the completed 3D MPA array [Fig. 2(f)]. Figures 2(g) and 2(h) show the scanning electron microscopy (SEM) images of the fabricated 3D MPA unit cell and array, respectively.

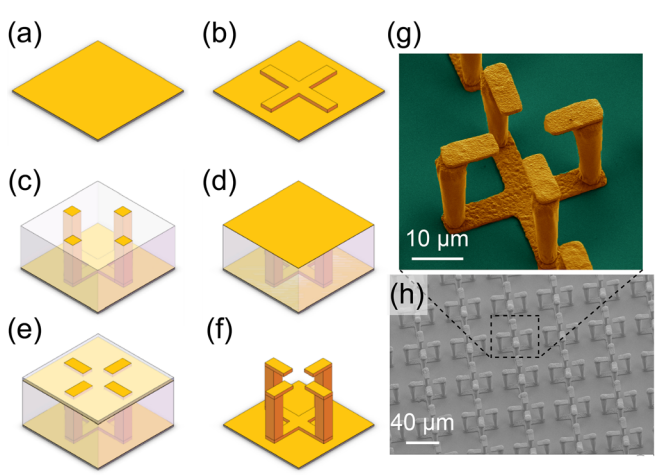

FIG. 2. (a)–(f) Depiction of the fabrication process of the 3D MPA unit cell. (g)–(h) Scanning electron microscopy (SEM) images of the fabricated 3D MPA. Zoom in (false color) reveals the details of the 3D MPA unit cell.

THz time domain spectroscopy (THz-TDS) was employed to characterize the 3D MPA in a normal incidence reflection configuration. We measured the reflection spectrum with the electric field of the THz pulse parallel with one of the top bars of the MPA [along the x-axis in Fig. 1(a)] to get the x-polarization response. Then, we rotated the sample by 90° to measure the y-polarization response at normal incidence. The experimental results for x- and y-polarized incident THz waves are presented in Figs. 3(a) and 3(b), in which the solid lines and dashed lines represent the experimentally measured and simulation results, respectively. Most importantly, the experimental results show a strong resonance at 1.65 THz and a high absorptivity of 99.6% with a quality factor Q of ~37 for x-polarization and y-polarization. The experimental results show excellent agreement with simulations. The slight mismatch between experimental results and simulation likely arises from imperfections in the fabrication process. In the experimental results, there are minor differences between x-polarization and y-polarization

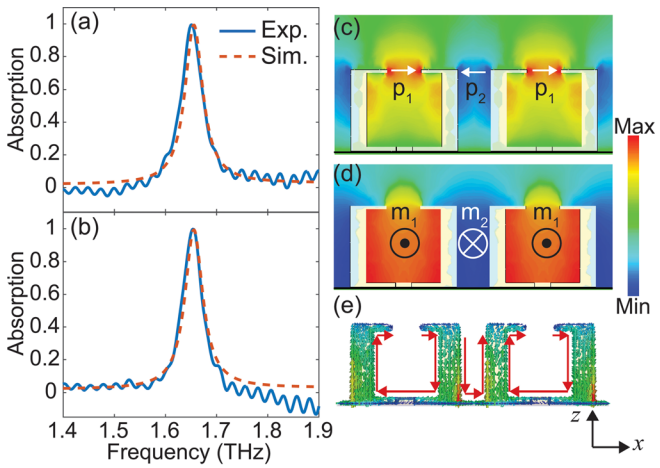

FIG. 3. (a) and (b) The experimental and simulated results for x- and y-polarized incident THz radiation, respectively. The solid lines represent experimental results, and the dashed lines represent simulations. Simulated electric (c) and magnetic (d) field magnitudes on resonance for x-polarization incidence. (e) The simulated surface electric current at the resonance frequency.

of 0.4% and 2% for the resonance frequency and quality factor, respectively. This discrepancy likely arises from the defects in the fabrication that may introduce some asymmetric errors in the structure. For our design, the resonance frequency and absorption are highly dependent on the dimensions of the two perpendicular stand-up SRRs in the unit cells. The oscillations in the off-resonance absorption arise from etalon reflections in the experiment.

In order to achieve a perfect absorption, the impedance of the MPA and the free space should be matched ($Z_{eff}=Z_0$). To better understand the origin of the absorption, we performed simulations to investigate the electromagnetic response at the unit cell level. In order to simplify the discussion, the incident THz wave is TE polarized [i.e., the electric field is polarized along the x-axis in Fig. 1(a)] without loss of generality. Figure 3(c) illustrates the electric field distribution of the 3D MPA in the middle plane of two neighboring unit cells at the resonance frequency. Electric dipoles in the capacitive gaps (p_1) and oppositely oriented dipoles between the adjacent unit cells (p_2) arise and largely determine the effective permittivity (ε_{eff}). In Fig. 3(d), the magnetic field distribution reveals that magnetic dipoles induced in the SRRs and, additionally, magnetic dipoles between neighboring SRRs give rise to the effective permeability (μ_{eff}). Hence, substantial flexibility in the design parameters is available for this structure such that the effective impedance matches the free-space impedance. The resonant surface current density is presented in Fig. 3(e). Besides the current oscillating in the SRRs, a current "links" neighboring unit cells. Thus, the resonance corresponds to a coupled LC resonance. The coupling between adjacent unit-cells indicates that not only the dimensions of the SRR unit cell influence the effective impedance of the 3D MPA but that the periodicity of the array also plays an important role. Therefore, a desired resonance frequency and absorption of a 3D MPA can be obtained by modifying the geometric dimensions of the SRRs and periodicity of the array.

According to the coupled mode theory,[25] the quality factor of a MPA is related to the ohmic loss and radiative losses, corresponding to the absorptive (Q_a) and radiative (Q_r) quality factors. In our 3D MPA, the ohmic losses occur solely in the metal since there is not any dielectric material present. Figure 3(e) shows the surface current density in the MPA, which demonstrates the energy loss distribution. Clearly, the electromagnetic energy is mainly absorbed by the pillars and the ground plane connecting pillars between neighboring unit cells. This modal current distribution leads to an absorptive quality factor $Q_a \sim 88.8$ according to the numerical simulations. The radiative quality factor is $\sim$75.2, estimated from the reflection coefficient and the total energy stored in the resonator.[25] The overall quality factor of the MPA is given by $Q=(Q_aQ_r)/(Q_a+Q_r)\approx 40.7$, in close agreement with the measured and simulated quality factors. Compared to the planar MPAs,[25] the absorptive quality factor is considerably larger due to the reduced absorptive losses achieved by eliminating the dielectric material as part of the absorber. We note that a high quality factor is preferred for sensing applications. For typical planar MPAs, the quality factors range from 5 to 22 in microwave,[12] terahertz,[6,25] and infrared[26] frequencies. Leveraging Fano resonances or higher-order resonance modes can increase the quality factor up to $\sim$34 in the terahertz regime.[27–29] However, such approaches may not be suitable for applications where single band absorption is required. Using superconducting materials as the metamaterial structure can significantly increase the quality factor[30] at the expense of having to remain below the superconducting transition temperature. A more detailed comparison of our results to the reported MPAs is listed in Table S1 in the supplementary material.

The impedance of the 3D MPA depends on the geometry and the surrounding dielectric environment. A sample with the photoresist (AZ9260) remaining, as illustrated in the inset of Fig. 4, was measured to investigate the change in the MPA absorption. From the experimental results shown in Fig. 4, we can see that there is a significant redshift of the resonance frequency (shifting from 1.65 THz to 1.16 THz) due to the presence of the photoresist. The absorption drops from 99.6% to 77.6%. The reason for the redshift is the change of the effective impedance of the MPA due to the larger dielectric constant of the photoresist in comparison to free space. According to the simulation results (dashed line in Fig. 4), modeling the photoresist as a dielectric with a permittivity of 2.8 and a loss tangent of 0.017 matches the experimental results. The optimal impedance match at the original resonance frequency is degraded with a suboptimal match established at the new resonant frequency. Besides the dielectric induced impedance mismatch, broadband absorption from the photoresist is evident. From Fig. 4, baseline absorption occurs in the simulation ($\sim$15%) and experiment ($\sim$20%). At the same time, the overall quality factor of the MPA is degraded to 13. In short, if the surrounding medium of the MPA is altered, the frequency, amplitude, and quality factor of the absorption spectrum will change. Thus, the 3D MPA could be useful in potential applications such as chemical/biological sensing.

From the discussion above, we can see that the simulation results have excellent agreement with the experimental results. Therefore, additional simulations have been employed to investigate other features of our 3D MPA that are difficult to measure with our THz-TDS reflection setup, as described in the supplementary material. The relevant simulation parameters can be found in Fig. 1. In this 3D MPA, a rotation symmetric unit cell structure, consisting of two orthogonally configured stand-up SRRs, is utilized to make it insensitive to the incident THz polarization. As the polarization angle of

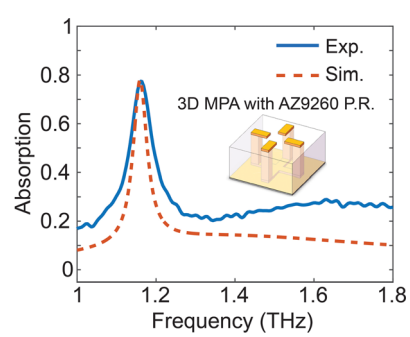

FIG. 4. (a) Experimental and simulated absorption spectra of the 3D MPA embedded in AZ9260 photoresist. Inset: the unit cell of the 3D MPA without removing the thick photoresist AZ9260, illustrated as a translucent cube.

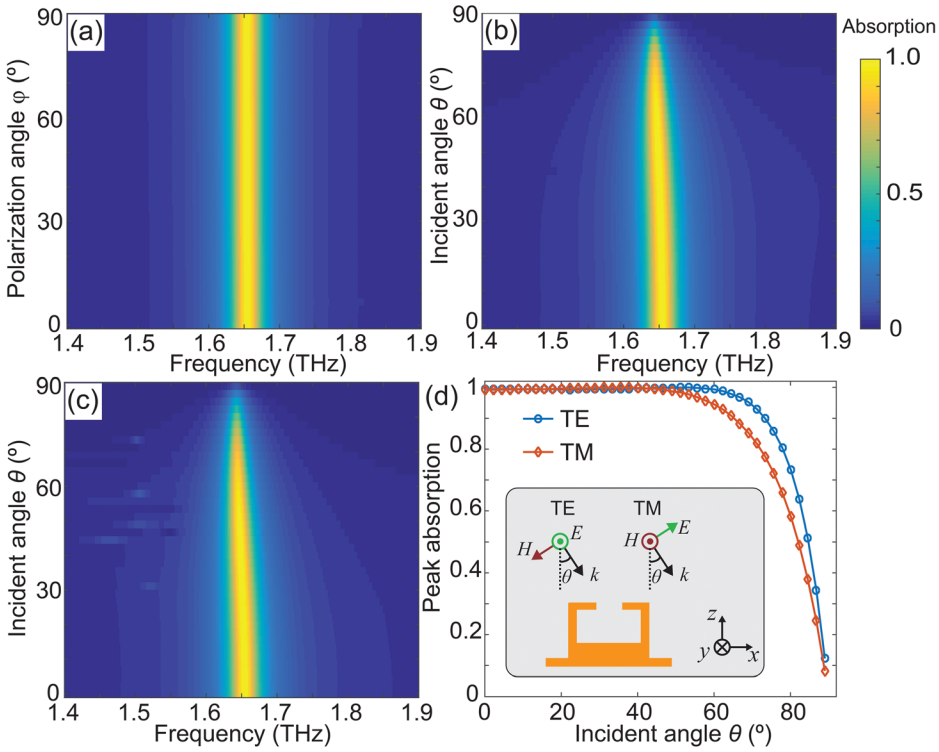

FIG. 5. (a) Simulation of the absorption spectra at different polarization angles: 0° is the TE mode and 90° is the TM mode. (b) and (c) The simulated absorption for TE and TM incident THz waves as the incident angle is swept from 0° to 89°. (d) Peak absorption of different incident angles at resonance for TE and TM polarization. Inset: the electric and magnetic field direction for TE and TM modes at different incident angles (θ).

incident THz wave changes from TE to TM at normal incidence, the resonance frequency and absorption should exhibit a negligible change. Figure 5(a) shows the simulated absorption spectra of the 3D MPA at various polarization angles from 0° (TE) to 90° (TM). The resonance frequency (1.65 THz) and absorption (99.9%) remain constant.

Achieving high absorption at various angles of incidence is also a noteworthy feature of this 3D MPA. The simulated absorption spectra at various angles of incidence for TE and TM polarizations are presented in Figs. 5(b) and 5(c), respectively. The expected peak absorption as a function of the angle of incidence (on resonance) for TE and TM polarizations is plotted in Fig. 5(d). The absorption remains above 90% as the incident angle increases from 0° to 60° for both TE and TM polarization. The absorption of TM polarization starts to drop significantly for larger incident angles, while the absorption for TE polarization incidence decreases gradually when the incident angle is larger than 70°. The absorption is larger than 50% for the incident angle up to 80°, indicating a wide-angle response of the 3D MPA. There is a slight difference in the incident angle dependency of the absorption for TE and TM polarization.

To conclude, we created a novel 3D terahertz MPA using a multilayer electroplating technique and surface micromachining. The unit cell of the 3D MPA consists of a copper ground plane and two orthogonal stand-up SRRs with the same geometric dimensions to form a symmetric structure. As opposed to conventional tri-layer planar MPAs, the dielectric spacer layer has been removed in order to eliminate the absorption of the spacer, leading to high-Q near-unity absorption. The three main factors that determine the effective medium impedance of the 3D MPA are geometric dimensions of the SRRs, the periodicity of the unit cells, and the dielectric response of the surrounding environment.

See supplementary material for the evaluation of the 3D metamaterial perfect absorber and details about terahertz time domain spectroscopy.

We acknowledge the National Science Foundation under Grant No. ECCS-1309835. In addition, we acknowledge support from DOE-Basic Energy Sciences under Grant No. DE-FG02-09ER46643. We thank Boston University Photonics Center for technical support. Meng Wu also acknowledges the fellowship support from China Scholarship Council (CSC).

[1]T. K. Todorov, K. B. Reuter, and D. B. Mitzi, Adv. Mater. **22**, E156 (2010).
[2]B. Shin, O. Gunawan, Y. Zhu, N. A. Bojarczuk, S. J. Chey, and S. Guha, Prog. Photovoltaics: Res. Appl. **21**, 72 (2013).
[3]N. Feng, D. Feng, S. Liao, X. Wang, P. Dong, H. Liang, C. Kung, W. Qian, J. Fong, R. Shafiiha, Y. Luo, J. Cunningham, A. Krishnamoorthy, and M. Asghari, Opt. Express **19**, 7062 (2011).
[4]Y. Hui and M. Rinaldi, Appl. Phys. Lett. **102**, 093501 (2013).
[5]N. P. Sergeant, M. Agrawal, and P. Peumans, Proc. SPIE **7410**, 74100C (2009).
[6]H. Tao, C. M. Bingham, A. C. Strikwerda, D. Pilon, D. Shrekenhamer, N. I. Landy, K. Fan, X. Zhang, W. J. Padilla, and R. D. Averitt, Phys. Rev. B **78**, 241103 (2008).
[7]D. Shrekenhamer, W.-C. Chen, and W. J. Padilla, Phys. Rev. Lett. **110**, 177403 (2013).
[8]F. Ding, Y.-X. Cui, X.-C. Ge, Y. Jin, and S.-L. He, Appl. Phys. Lett. **100**, 103506 (2012).
[9]S. Liu, H. Chen, and T.-J. Cui, Appl. Phys. Lett. **106**, 151601 (2015).
[10]T. Kampfrath, K. Tanaka, and K. A. Nelson, Nat. Photonics **7**, 680 (2013).
[11]M. Walther, B. M. Fischer, A. Ortner, A. Bitzer, A. Thoman, and H. Helm, Anal. Bioanal. Chem. **397**, 1009 (2010).
[12]N. I. Landy, S. Sajuyigbe, J. J. Mock, D. R. Smith, and W. J. Padilla, Phys. Rev. Lett. **100**, 207402 (2008).
[13]C. M. Watts, X. Liu, and W. J. Padilla, Adv. Mater. **24**, OP98 (2012).
[14]W.-C. Chen, A. Cardin, M. Koirala, X. Liu, T. Tyler, K. G. West, C. M. Bingham, T. Starr, A. F. Starr, N. M. Jokerst, and W. J. Padilla, Opt. Express **24**, 6783 (2016).
[15]X. Xiong, S.-C. Jiang, Y.-H. Hu, R.-W. Peng, and M. Wang, Adv. Mater. **25**, 3994 (2013).
[16]F. Ma, Y.-S. Lin, X. Zhang, and C. Lee, Light Sci. Appl. **3**, e171 (2014).

[17]K. Aydin, I. Bulu, K. Guven, M. Kafesaki, C. M. Soukoulis, and E. Ozbay, New J. Phys. **7**, 168 (2005).
[18]H.-T. Chen, Opt. Express **20**, 7165 (2012).
[19]Y. Wen, W. Ma, J. Bailey, G. Matmon, G. Aeppli, and X. Yu, Appl. Phys. Lett. **105**, 141111 (2014).
[20]L. Huang, D. R. Chowdhury, S. Ramani, M. T. Reiten, S.-N. Luo, A. K. Azad, A. J. Taylor, and H.-T. Chen, Appl. Phys. Lett. **101**, 101102 (2012).
[21]H. R. Seren, G. R. Keiser, L. Cao, J.-D. Zhang, A. C. Strikwerda, K.-B. Fan, G. D. Metcalfe, M. Wraback, X. Zhang, and R. D. Averitt, Adv. Opt. Mater. **2**, 1221 (2014).
[22]K. Fan, X. Zhao, J. Zhang, K. Geng, G. R. Keiser, H. R. Seren, G. D. Metcalfe, M. Wraback, X. Zhang, and R. D. Averitt, IEEE Trans. Terahertz Sci. Technol. **3**, 702 (2013).
[23]X. Zhao, K. Fan, J. Zhang, H. R. Seren, G. D. Metcalfe, M. Wraback, R. D. Averitt, and X. Zhang, Sens. Actuators, A **231**, 74 (2015).
[24]K. Fan, A. C. Strikwerda, H. Tao, X. Zhang, and R. D. Averitt, Opt. Express **19**, 12619 (2011).
[25]C. Qu, S. Ma, J. Hao, M. Qiu, X. Li, S. Xiao, Z. Miao, N. Dai, Q. He, S. Sun, and L. Zhou, Phys. Rev. Lett. **115**, 235503 (2015).
[26]N. Liu, M. Mesch, T. Weiss, M. Hentschel, and H. Giessen, Nano Lett. **10**, 2342 (2010).
[27]I. Al-Naib, R. Singh, C. Rockstuhl, F. Lederer, S. Delprat, D. Rocheleau, M. Chaker, T. Ozaki, and R. Morandotti, Appl. Phys. Lett. **101**, 071108 (2012).
[28]S. Yu, X. Piao, J. Hong, and N. Park, Phys. Rev. A **92**, 011802 (2015).
[29]B.-X. Wang, X. Zhai, G.-Z. Wang, W.-Q. Huang, and L.-L. Wang, J. Appl. Phys. **117**, 014504 (2015).
[30]B. Jin, C. Zhang, S. Engelbrecht, A. Pimenov, J. Wu, Q. Xu, C. Cao, J. Chen, W. Xu, L. Kang, and P. Wu, Opt. Exp. **18**, 17504 (2010).